Analytical study of in-situ combustion in a wet porous medium.

Mailybaev, A.A.* Bruining, J.,† Chapiro, G.,‡
and Marchesin, D.§

Key words: *in-situ combustion, Riemann problem, Arrhenius' law.*

Abstract

There is renewed interest using combustion for the recovery of medium viscosity oil. In this analytical study we take into account the reaction occurring between the residual petroleum coke and the oxygen contained in the injected air. We also assume the presence of a small amount of immobile liquid phase, which can evaporate. This study can be applied to the recovery of medium and heavy oil off-shore.

Physically, we consider a tube of homogeneous porous medium insulated from the sides with no thermal or gas flow through the boundary. We neglect the heat capacity of the gas and liquid phases relative to the rock. The temperature is the same for rock and all phases. Pressure decline along the tube is ignored.

The resulting 1-D physical model is described by a system of balance equations with diffusion and heat conduction for enthalpy, gas components, fuel and liquid concentrations. The reaction rate is given by a first order mass action law and Arrhenius' law. The evaporation rate is described by the Clausius-Clapeyron relation; ideal gas behavior is assumed.

The Riemann problem for this system is solved assuming that the reaction and evaporation occur inside vertical layers with finite width. The internal structure of the combustion front was obtained together with the speeds and the characteristic length of the waves. This method is used in the literature but it lies outside the scope of standard fractional flow theory. We compare this solution with the exact solution obtained for the same system without the liquid phase. Both solutions are discussed from a physical point of view and confirmed by numerical simulations.

*Inst. of Mechanics, Moscow State Univ., Moscow, Russia. mailybaev@imec.msu.ru
†Department of Geo Technology, TU Delft, Delft, The Netherlands. j.bruining@tudelft.nl
‡IMPA, Rio de Janeiro, Brazil. grigori@fluid.impa.br
§IMPA, Rio de Janeiro, Brazil. marchesi@fluid.impa.br

1 Introduction

Huge deposits of difficult oil that cannot be recovered by conventional means have renewed interest in heavy oil recovery techniques such as in situ combustion (ISC). ISC is more energy efficient than steam injection as the CO_2 is produced in-situ. Besides, the Brazilian oil is most part off-shore and steam injection to the bottom presents technical difficulties such as heat losses. This technique involves the injection of air, or air enriched with oxygen or nitrogen to enable combustion of oil and other consecutive reactions within the reservoir formation, leading to the release of heat. Conducted heat ahead of the combustion front, reduces the oil viscosity and leads to in situ distillation (upgrading). Carbon dioxide created during combustion can also assist in the recovery by increasing pressure and by mixing with the oil, reducing its viscosity and enhancing flow (see [4, 12]).

The primary limitation of ISC is that the combustion front is hard to control. It is asserted that understanding the mechanism will help to develop procedures for improve control.

We use the schematic division of the ISC processes shown in Figure 1, see [9]. Following the counter current flow direction (right to left or from the production to the injection well) we can separate the ISC process in the light hydrocarbons (HC) zone, the steam zone, the cracking zone, the coke formation zone and the coke combustion zone.

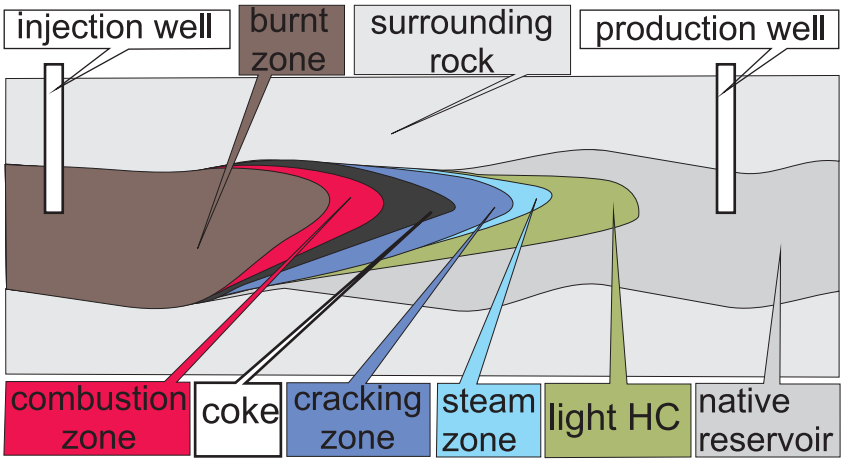

Figure 1: Schematic representation of ISC process.

Condensation of all light oil that evaporated elsewhere occurs inside the light hydrocarbon zone. In addition to initial water in the reservoir, which evaporates due to high temperature, water is also a combustion product. This water condenses mainly downstream of the steam zone situated downstream of the combustion process. Heat released during condensation elevates the reservoir temperature and increases the evaporation of light oil components.

Continuing upstream we find the cracking zone, where visbreaking and coking stages [1] occur, and the coke zone, containing only coke, which is consumed inside the combustion zone.

Inside the combustion zone the residual coke reacts with the injected oxygen. The micro-porous structure of coke and related parameters, such as reactive area of coke particles and transport of oxygen into the pores, are important to describe this process, see [5]. There is abundant literature, for example [2], focusing on the reaction kinetics of petroleum coke.

In this text we do not study the cracking processes that occur inside the cracking zone and study the interaction of the evaporation zone and combustion zone only.

In Section 2 we introduce the physical model describing combustion-vaporization in porous media and obtain its dimensionless form. In Section 3 we present the wave sequences for the wet combustion model. Next, in Section 4 we show numerical experiments supporting our analysis. Finally, in Section 5 we find the approximate analytical solution for dry combustion model and compare it to combustion-vaporization model. We end with some conclusions.

2 Wet combustion model

Consider a horizontal porous rock cylinder thermally insulated and filled with gas, vaporizable liquid and combustible solid fuel. We will study flows possessing a combustion wave in the case when the oxidizer (air with oxygen) is injected in the porous medium that contained initially a liquid and a non-reactive gas besides the solid fuel. We assume that the amount of liquid is small, so its mobility is negligible. We assume that only a small part of the available space is occupied by the solid fuel and the liquid, so that we can neglect changes of porosity in the reaction, evaporation and condensation processes. We assume that the temperature of solid, liquid and gas is the same (local thermal equilibrium).

The heat transport equation is, [7]:

$$C_m \frac{\partial T}{\partial t} + \frac{\partial c_g \rho u (T - T_{res})}{\partial x} = \lambda \frac{\partial^2 T}{\partial x^2} + Q_r W_r - Q_e W_e, \tag{1}$$

where T [K] is the temperature, T_{res} is the initial reservoir temperature, ρ [mole/m^3 of gas] is the *molar* density of the gas mixture, u [m/s] is the Darcy velocity, C_m [J/m^{3}K] is the heat capacity of the rock matrix per unit volume of porous medium, c_g [J/mole K] is the heat capacity of gas per mole, λ [J/smK] is the thermal conductivity of the porous medium, Q_r, Q_e [J/mole] are the heats (enthalpies) of combustion and evaporation of the solid and the liquid at the reservoir temperature T_{res}, and W_r, W_e [mole/m^{3}s] are the reaction and evaporation rates.

We consider a single component liquid, vaporizable oil. We denote by X its vapor molar fraction in the gas phase (mole of vapor/mole of gas). The gas has several components: vapor, oxygen and passive (inert and combusted) gas. We denote the molar fractions of oxygen and passive gas in the gas-phase by Y and Z respectively. Then, we write the mass balance equations for the components X, Y, Z as (see e.g. [6]):

$$\varphi \frac{\partial X \rho}{\partial t} + \frac{\partial X \rho u}{\partial x} = D \varphi \frac{\partial}{\partial x} \rho \frac{\partial X}{\partial x} + W_e, \tag{2}$$

$$\varphi \frac{\partial Y \rho}{\partial t} + \frac{\partial Y \rho u}{\partial x} = D \varphi \frac{\partial}{\partial x} \rho \frac{\partial Y}{\partial x} - \mu_o W_r, \tag{3}$$

$$\varphi \frac{\partial Z \rho}{\partial t} + \frac{\partial Z \rho u}{\partial x} = D \varphi \frac{\partial}{\partial x} \rho \frac{\partial Z}{\partial x} + \mu_g W_r, \tag{4}$$

where φ is the porosity, and D [m^2/s] is the diffusion coefficient for vapor, oxygen and passive gas in the gaseous phase; they are taken to be equal for simplicity. We assume that $D \approx 2 \cdot 10^{-5}$ [m^2/s] at P_{atm}; D is inversely proportional to the pressure [5]. Using that the sum of mole fractions $X + Y + Z$ is equal to one, we obtain the mass balance equation for the total gas:

$$\varphi \frac{\partial \rho}{\partial t} + \frac{\partial \rho u}{\partial x} = (\mu_g - \mu_o) W_r + W_e. \tag{5}$$

As the solid fuel and the liquid do not move, their concentrations satisfy the equations for reaction and evaporation, respectively:

$$\frac{\partial n_f}{\partial t} = -\mu_f W_r, \tag{6}$$

$$\frac{\partial n_l}{\partial t} = -W_e, \tag{7}$$

where n_f, n_l [mole/m^3 of porous medium] are the molar concentrations of solid fuel and liquid. In the combustion reaction, μ_f moles of solid fuel react with μ_o moles of oxygen and generate μ_g moles of gaseous products. Below we assume that the stoichiometric coefficients are $\mu_f = \mu_o = \mu_g = 1$, as in the reaction $C + O_2 \to CO_2$.

The ideal gas law for the gaseous phase has the form

$$P_{tot} = \rho R T \tag{8}$$

with the ideal gas constant $R = 8.314$ [J/mole K] and the prevailing pressure P_{tot} [Pa]. Assuming that the variation of pressure is small, we take $P_{tot} = const$, thus disregarding the pressure gradient caused by the flow of gases. The vapor pressure in thermodynamic equilibrium with the liquid is described by the Clausius-Clapeyron relation

$$P_X = P_{atm} \exp\left(-\frac{Q_e}{R} \left(\frac{1}{T} - \frac{1}{T_b} \right) \right), \tag{9}$$

valid in the region containing a pure liquid, where T_b is the normal liquid boiling temperature at atmospheric pressure and $P_X = X_{eq} P_{tot}$ is the partial pressure of oil vapor in equilibrium with liquid oil at the temperature T. With the ideal gas law we can express the equilibrium mole fraction of vapor X_{eq} as

$$X_{eq}(T) = \frac{P_X}{P_{tot}} = \frac{P_{atm}}{P_{tot}} \exp\left(-\frac{Q_e}{R} \left(\frac{1}{T} - \frac{1}{T_b} \right) \right). \tag{10}$$

The evaporation (condensation) rate can be taken as $W_e = k n_l (X_{eq}(T) - X)$, where the equilibrium vapor fraction $X_{eq}(T)$ is computed by (10). The coefficient k can be different for $X > X_{eq}$ and $X < X_{eq}$. Below we will assume that k is large, so that liquid and vapor are always in equilibrium: $X \approx X_{eq}(T)$.

We use the Arrhenius law and the first order law of mass action in the reaction rate

$$W_r = K_r Y n_f \exp\left(-E_r/(RT)\right) \tag{11}$$

with the constant activation energy E_r [J/mole] and the pre-exponential parameter K_r [1/s], which is also assumed to be constant.

The variables to be found are the temperature T, the molar concentrations of solid fuel n_f and liquid n_l, the molar fractions of oxygen and vapor Y, X, and the Darcy velocity u. The coefficients φ, C_m, c_g, λ, D, Q_r, Q_e are assumed to be constant (neglecting the dependence on temperature and gas composition).

2.1 Dimensionless equations. The equations are non-dimensionalized [14] by introducing dimensionless dependent and independent variables (denoted by tildes) as a ratio of the dimensional quantities and reference quantities (denoted by stars):

$$\tilde{t} = \frac{t}{t^*},\ \ \tilde{x} = \frac{x}{x^*},\ \ \theta = \frac{T - T_{res}}{T^*},\ \ \tilde{\rho} = \frac{\rho}{\rho^*},\ \ \tilde{n}_{f,l} = \frac{n_{f,l}}{n^*_{f,l}},\ \ \tilde{u} = \frac{u}{u^*}. \tag{12}$$

Let us take $v^* = c_g \rho^* u_{inj}/C_m$, which turns out to be the speed of the thermal wave (a wave where temperature changes with no reaction). Then we introduce the reference length and time as $x^* = \lambda/(C_m v^*)$ and $t^* = x^*/v^*$, which are appropriate for the thermal wave. The temperature change for combustion under adiabatic conditions can be used as the characteristic temperature $T^* = Q_r n_f^*/C_m$. Thus, our choice for reference quantities is

$$t^* = \frac{x^*}{v^*},\ x^* = \frac{\lambda}{C_m v^*},\ T^* = \frac{Q_r n_f^*}{C_m},\ \rho^* = \frac{P_{tot}}{RT_{res}},\ v^* = \frac{c_g \rho^* u_{inj}}{C_m},\ n^*_{f,l} = n^{res}_{f,l},\ u^* = u_{inj}, \tag{13}$$

where T_{res} and $n^{res}_{f,l}$ are the initial reservoir temperature and fuel, liquid concentrations, respectively, and u_{inj} is the gas injection velocity. Using (12), (13) and omitting the tildes, equations (1)–(10) are written in dimensionless form as

$$\frac{\partial \theta}{\partial t} + \frac{\partial \rho u \theta}{\partial x} = \frac{\partial^2 \theta}{\partial x^2} + w_r - \beta w_e, \tag{14}$$

$$\frac{\partial \rho}{\partial t} + \sigma \frac{\partial \rho u}{\partial x} = \gamma_l w_e, \tag{15}$$

$$\frac{\partial Y \rho}{\partial t} + \sigma \frac{\partial Y \rho u}{\partial x} = \frac{1}{Le} \frac{\partial}{\partial x} \rho \frac{\partial Y}{\partial x} - \gamma_f w_r, \tag{16}$$

$$\frac{\partial X \rho}{\partial t} + \sigma \frac{\partial X \rho u}{\partial x} = \frac{1}{Le} \frac{\partial}{\partial x} \rho \frac{\partial X}{\partial x} + \gamma_l w_e, \tag{17}$$

$$\frac{\partial n_f}{\partial t} = -w_r, \tag{18}$$

$$\frac{\partial n_l}{\partial t} = -w_e, \tag{19}$$

$$\rho(\theta + \theta_0) = \theta_0, \tag{20}$$

$$X_{eq} = \alpha \exp\left(-\frac{h}{\theta + \theta_0}\right) \tag{21}$$

with dimensionless constants

$$\begin{gathered} Le = \frac{\lambda}{C_m D},\ N_{Da} = K_r t^*,\ \gamma_{f,l} = \frac{n^*_{f,l}}{\varphi \rho^*},\ \sigma = \frac{u^*}{\varphi v^*},\ \beta = \frac{Q_e n^*_l}{Q_r n^*_f}, \\ h = \frac{Q_e}{RT^*},\ \mathcal{E} = \frac{E}{RT^*},\ \kappa = t^* k,\ \theta_0 = \frac{T_{res}}{T^*},\ \alpha = \frac{P_{atm}}{P_{tot}} \exp\left(\frac{Q_e}{RT_b}\right). \end{gathered} \tag{22}$$

Here Le is the Lewis number; N_{Da} is the Damkohler number; $\gamma_{f,l}$ characterizes the initial fuel and liquid concentrations relative to the gas density; σ is the interstitial gas velocity relative to the thermal wave velocity; β gives the ratio of evaporation and combustion heats for total amounts of liquid and fuel, etc.. We omitted equation (4) as $Z = 1 - X - Y$.

The dimensionless reaction and evaporation rates are given by $w_r = t^* W_r / n^*_f$ and $w_e = t^* W_e / n^*_l$. The evaporation rate takes the form

$$w_e = \kappa n_l (X_{eq}(\theta) - X). \tag{23}$$

For the reaction rate (11), we get the dimensionless expression

$$w_r = N_{Da} Y n_f \exp\left(-\mathcal{E}/(\theta + \theta_0)\right). \tag{24}$$

In order to study solution of the system (14)-(21) in form of traveling waves we assume that the solution depend on the traveling variable $\xi = x - Vt$, where V is the constant traveling wave speed, i.e., either $V = v_T$, $V = v_R$ or $V = v_C$ as shown in Fig. 2. We rewrite the equations (14)-(19) is this traveling form, obtaining:

$$-V\theta' + (\rho u \theta)' = \theta" + w_r - \beta w_e, \tag{25}$$

$$-V\rho' + \sigma(\rho u)' = \gamma_l w_e, \tag{26}$$

$$-V(Y\rho)' + \sigma(Y\rho u)' = (\rho Y')'/L_e - \gamma_f w_r, \tag{27}$$

$$-V(X\rho)' + \sigma(X\rho u)' = (\rho X')'/L_e + \gamma_l w_e, \tag{28}$$

$$-V n'_f = -w_r, \tag{29}$$

$$-V n'_l = -w_e, \tag{30}$$

where $()'$ means $d/d\xi()$. The equations (20) and (21) remain the same in the traveling form.

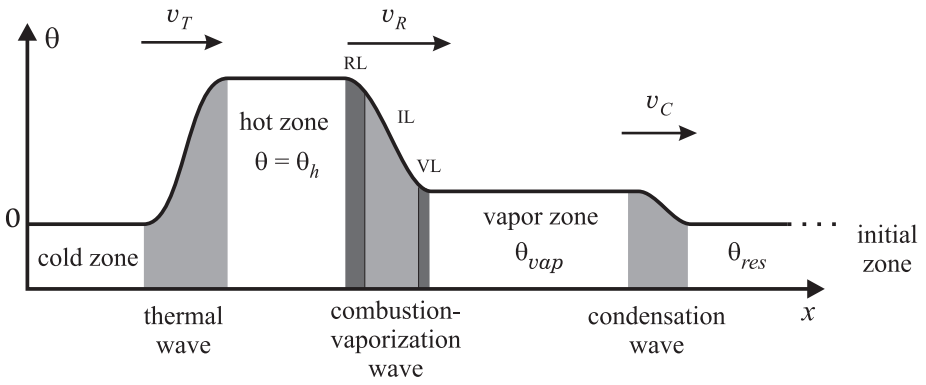

Figure 2: Wave sequence for complete fuel consumption.

3 Wave sequence for complete fuel consumption

In this section, we study the solution having a structure shown in Fig. 2. The solution consists of three waves a slow thermal wave, a medium combustion-vaporization wave and a fast condensation wave. These waves are separated by zones with constant states.

In the thermal wave the temperature raises to a high value θ_h. Ahead of this wave, there is a constant hot zone. The combustion-vaporization wave consists of combustion and vaporization layers joined by an intermediate layer. Upstream the combustion layer, the reaction stops due to lack of fuel (*complete fuel consumption*). Ahead of the combustion layer, the reaction does not start because the reaction rate is negligible at low temperature. We will see that, under rather general conditions (explicitly specified), all the liquid evaporates in the vaporization layer, and none of its vapor remains in the reaction area.

The zone ahead of the combustion-vaporization wave contains liquid in equilibrium with its vapor in the transported gas. This zone ends with a condensation wave. There is also a fourth composition wave that travels with the speed of the gas, which is much larger than the speeds of the other waves, so that this wave does not appear in Fig. 2 and will be ignored. Along this wave, the concentrations of unburned oxygen and of produced gases drop to zero, while the temperature and total gas flux do not change. To the right of this wave, we have the gas at initial reservoir composition, as well as initial reservoir liquid.

The boundary conditions at the left injection side determine the temperature, gas flux and oxygen concentration:

$$x = 0,\ t \geq 0: \quad \theta = 0, \quad \rho = u = 1, \quad Y_{inj}, \quad X = 0, \tag{31}$$

where we assumed that the injected gas temperature is equal to the initial reservoir temperature. The last condition in (31) means that there is no vapor in the injected gas. The initial data in the reservoir determine the temperature, fuel and liquid concentrations at the downstream end

$$t = 0: \quad \theta = 0,\ n_f = n_l = 1,\ X_{res} = \alpha \exp\left(-h/\theta_0\right). \tag{32}$$

where X_{res} is determined by (21) by replacing θ by zero.

Complete fuel consumption implies that the condition $n_f = 0$ holds behind the combustion-vaporization wave. Complete oxygen consumption is not required ahead of the combustion-vaporization wave, and the concentration of unburned oxygen is denoted by Y_{unb}. No liquid nor vapor is left behind this wave: $n_l = X = 0$.

3.1 Thermal wave. Since neither vapor, liquid nor fuel are left behind the combustion-vaporization wave, we have $X = n_l = n_f = 0$. The oxygen concentration $Y = Y_{inj}$ does not change in the thermal wave (the corresponding equation (16) is trivially satisfied). Notice that the gas speed u was scaled in (12) in such way that the thermal wave speed is $v_T = 1$. The thermal wave is described by the equations (25) and (26) substituting the wave speed V by v_T. Let θ_h be the temperature of the hot zone, see Fig. 3. We solve (25)-(26) with θ tending to zero as $x \to -\infty$, to θ_h as $x \to \infty$, obtaining:

$$\theta(t,x) = \frac{\theta_h}{2} + \frac{\theta_h}{2}\,\mathrm{erf}\left(\frac{x - x_T - v_T t}{2\sqrt{t}}\right), \quad v_T = 1, \tag{33}$$

where x_T is the wave position at $t = 0$, and $\mathrm{erf}(x) = (2/\sqrt{\pi})\int_0^x e^{-\xi^2} d\xi$ is the error function; recall that $\mathrm{erf}(\infty) = -\mathrm{erf}(-\infty) = 1$. The dimensional speed v^* given in (13) is the thermal wave speed. The width of the wave grows proportionally to $\sqrt{t}$ due to heat conduction. The values of the variables in the hot zone are given by their values at the right-hand side of the thermal wave:

$$\text{Hot zone}: \quad \theta = \theta_h, \;\; \rho u = 1, \;\; Y = Y_{inj}, \;\; X = n_f = n_l = 0, \tag{34}$$

where θ_h is unknown. From (20), we also find $\rho = 1/u = \theta_0/(\theta_h + \theta_0)$.

3.2 Combustion-vaporization wave. According to the wave structure in Fig. 2, we conjecture that the reaction and vaporization take place in a single traveling wave. The wave travels with speed v_R and consists of a reaction layer (RL) and a vaporization layer (VL), joined by an intermediate layer (IL). In the RL, the solid fuel reacts with oxygen: $w_r > 0$, $w_e = 0$. In the VL, the liquid vaporizes: $w_r = 0$, $w_e > 0$. Finally, in the IL we have $w_r = w_e = 0$. The combustion-vaporization wave is faster than the thermal wave, which implies that $v_R > 1$.

Let us introduce the traveling coordinate $\xi = x - x_R - v_R t$, where x_R is the wave position at $t = 0$. We choose the origin such that the RL, IL and VL correspond to $\xi < 0$, $0 < \xi < L$ and $\xi > L$, respectively. All the state variables in the wave depend only on ξ; the prime will denote the derivative with respect to ξ. On the ends of the wave ($\xi \to \pm\infty$), the derivatives with respect to ξ vanish. We study first the RL and VL, and afterwards patch them through the IL.

3.2.1 Reaction layer. In the RL, there is neither liquid nor vapor, equations (25)–(30) were solved in [7] using ($n_l = X = w_e = 0$) for two extreme cases that are easily accessible for an analytical approach: (a) when the diffusion term $Le\, l_R \sigma$ is small, and (b) when it is dominant:

$$(a): \;\; Le\, l_R \sigma \gg 1, \qquad (b): \;\; Le\, l_R \sigma \ll 1; \tag{35}$$

the explicit expression for l_R is found below, see (39).

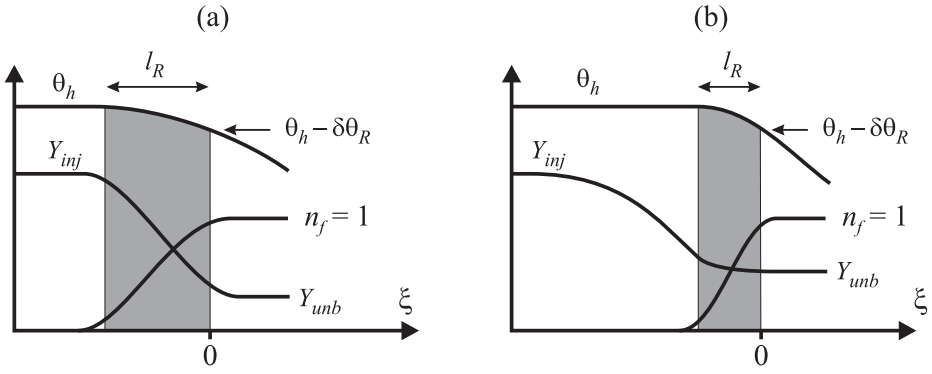

Figure 3: Schematic structure of the reaction layer (RL) for small diffusion (a) and dominant diffusion (b).

We assume that the reaction does not start ahead of the RL because the temperature is low (despite the presence of both fuel and oxygen). Strictly speaking, the RL does not have a sharp border, but rather there is a continuous passage from the RL to the IL. We can find an approximate analytical solution for the RL, which later must be patched with the solution in the IL.

For case (a), the mass diffusion term is small and can be neglected. Again in the absence of the evaporation Eq. (26) gives $\rho u = 1$. Then we use the Eq. (27) to isolate the term w_r and substitute it into Eq. (25). After integration and some simplifications involving tedious algebra, we arrive at an implicit expression for the temperature inside the RL:

$$(a): \quad \frac{(\theta_h + \theta_0)^2}{\mathcal{E}} \exp\left(-\frac{\mathcal{E}}{\theta_h + \theta_0}\right) = \frac{v_R \sigma}{N_{Da} \gamma_f} \log \frac{Y_{inj}}{Y_{unb}}. \tag{36}$$

The fraction of unburned oxygen in the gas ahead of the RL is:

$$Y_{unb} = Y_{inj} - v_R \gamma_f / \sigma. \tag{37}$$

For the case (b), we take approximately $Y = const$ inside RL; this constant must be equal to the amount of unburned oxygen Y_{unb} ahead of the RL. A similar analysis leads to an implicit expression for the temperature inside the RL:

$$(b): \quad \frac{(\theta_h + \theta_0)^2}{\mathcal{E}} \exp\left(-\frac{\mathcal{E}}{\theta_h + \theta_0}\right) = \frac{v_R^2}{N_{Da} Y_{unb}}. \tag{38}$$

Fig. 3 shows the structures of the RL in the cases (a) and (b).

Using equations (36) and (38) one can obtain [7] the effective temperature variation $\delta\theta_R$ across the RL for both cases (a) and (b) and the effective (dimensionless) length can be approximated by, see Fig 3:

$$\delta\theta_R \approx (\theta_h + \theta_0)^2 / \mathcal{E}, \quad l_R \sim 2\delta\theta_R / v_R \approx 2(\theta_h + \theta_0)^2 / (v_R \mathcal{E}). \tag{39}$$

We set the traveling coordinate origin $\xi = 0$ at the right-hand side of the RL. As the temperature variation is small across the RL, we assume that $\theta \approx \theta_h$ upstream of the RL. Using Eqs. (26) and (37) we obtain at $\xi = 0$:

$$\xi = 0: \ \theta = \theta_h, \ \theta' = -v_R, \ \rho u = 1, \ X = 0, \ Y_{unb} = Y_{inj} - v_R \gamma_f/\sigma, \ n_f = 1, \ n_l = 0. \quad (40)$$

The condition $n_l = 0$ (no liquid) follows from the assumption that $\theta > \theta_b$. For $\xi > 0$ we will neglect the oxidation reaction, as its rate is very small at low temperatures.

3.2.2 Intermediate layer. The IL lies in the interval $0 < \xi < L$. In the IL, there is neither reaction nor vaporization: $w_r = w_e = 0$, and the gas flux is constant $\rho u \equiv 1$. Using these simplifications in Eq. (25) we find general solution for the temperature inside the IL:

$$\theta = \theta_h - \frac{v_R}{A} + \frac{v_R}{A} \exp(-A\xi), \quad A = v_R - 1 > 0. \quad (41)$$

Denoting the values of θ and θ' at $\xi = L$ by θ_L and θ'_L, and using (41) we get:

$$\theta_L = \theta_h - \frac{v_R}{A}(1 - e^{-AL}), \quad \theta'_L = -v_R e^{-AL}. \quad (42)$$

Using $\rho u = 1$ and $w_e = 0$ in Eq. (28) we integrate it twice taking into account that the vapor concentration tends to zero on the left ($X = X' = 0$ at $\xi = 0$) and using the condition $X = X_L$ at $\xi = L$ obtaining:

$$X = X_L \exp\left(- \int_\xi^L \frac{\sigma \, Le(\theta + \theta_0)}{\theta_0} d\xi \right). \quad (43)$$

3.2.3 Vaporization layer. The VL starts at $\xi = L$, see Fig 4. Inside the VL, we have $w_e > 0$ and $w_r = 0$. We study the VL assuming that the temperature variation $\delta\theta$ in the layer is small, so that $\theta \approx \theta_{vap}$. Substituting w_e from (23) into (25)-(27) and integrating over VL we obtain:

$$\delta(\theta')_V - \beta v_R n_l^{vap} = 0, \quad (44)$$

$$\delta(\rho u)_V - \gamma_l v_R n_l^{vap} = 0, \quad (45)$$

$$\frac{\rho_{vap}}{Le} \delta(X')_V - \sigma \delta(X \rho u)_V + \gamma_l v_R n_l^{vap} = 0, \quad (46)$$

where $\rho_{vap} = \theta_0/(\theta_{vap} + \theta_0)$ and $\delta()_V$ denotes the change of the quantity across the VL; we took into account that $[n_l] = n_l^{vap}$ is the liquid concentration ahead of the wave.

Ahead of the VL (in the vapor zone) we have $\theta' = 0$, $\rho u = (\rho u)_{vap}$, $X = X_{vap}$ and $X' = 0$. Behind the VL, $\theta' = \theta'_L$, $\rho u = 1$, $X = X_L$ and $X' = X'_L$. Expression (43) gives $X'_L = Le \, \sigma X_L/\rho_{vap}$. Along the VL we have $\theta \approx \theta_{vap}$. Using all these conditions in (44)–(46), some calculations yield behind the VL:

$$\xi = L: \ \ \theta = \theta_{vap}, \ \ \theta' = -\beta v_R n_l^{vap}; \quad (47)$$

and ahead of the VL (i.e., in the vapor zone):

$$(\rho u)_{vap} = 1 + \gamma_l v_R n_l^{vap}/\sigma, \ \ X_{vap} = (1 + \sigma/(\gamma_l v_R n_l^{vap}))^{-1}. \quad (48)$$

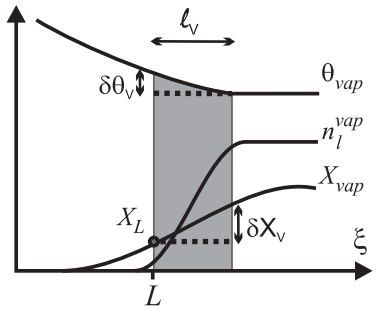

Figure 4: Schematic structure of the vaporization layer (VL), which is colored in gray.

Using (47) with $A = v_R - 1$ in (42) yields the expression for θ_{vap} and the IL length L:

$$\theta_{vap} = \theta_h - \frac{v_R(1 - \beta n_l^{vap})}{v_R - 1}, \quad L = -\frac{\log(\beta n_l^{vap})}{v_R - 1}. \tag{49}$$

The equilibrium condition (21) in the vapor zone reads

$$X_{vap} = \alpha \exp\left(-h/(\theta_{vap} + \theta_0)\right). \tag{50}$$

Since we neglect the oxidation in the IL and VL, the oxygen flux is constant in the traveling frame in these layers. The mole fraction of oxygen inside the vapor zone ahead of the combustion-vaporization wave can be computed from the condition $Y_{vap}(\rho u)_{vap} = Y_{unb}$, where $(\rho u)_{vap}$ is given in (48).

Let us estimate the VL structure parameters, assuming that the two terms on the right-hand side of each of equations (25) and (28) are of same order. Comparing these terms and using (23), we find $\delta\theta_V/l_V^2 \sim \beta\kappa\,\delta X_V$ and $1/(l_V^2 Le) \sim \gamma_l\kappa$, and l_V is the effective length of the VL (see Fig 4). From (30) we obtain $v_R/l_V \sim \kappa\,\delta X_V$. Expressing l_V from the second relation, and then δX_V and $\delta\theta_V$ from the third and first relations we derive the estimates :

$$\delta\theta_V \sim \frac{\beta v_R}{\sqrt{Le\,\gamma_l\kappa}}, \quad l_V \sim \frac{1}{\sqrt{Le\,\gamma_l\kappa}}, \quad \delta X_V \sim v_R\sqrt{\frac{Le\,\gamma_l}{\kappa}}. \tag{51}$$

3.2.4 Defining equations. Here we summarize the equations for the combustion-vaporization wave. There are six defining equations: (37), (48), (49), (50) and, depending on the case, (36) or (38). They relate the values of seven unknown variables: θ_h, θ_{vap}, X_{vap}, Y_{unb}, n_l^{vap}, $(\rho u)_{vap}$ and the wave speed v_R. These equations are analogous to Rankine-Hugoniot conditions; they result from the study of the wave structure.

3.3 Condensation wave. The vapor zone (see Fig. 2) between the combustion-vaporization wave and condensation wave contains liquid with concentration $n_l = n_l^{vap}$ in equilibrium with vapor at concentration X_{vap}, which is related to θ_{vap} by (21). The condensation wave travels with speed v_C. Solving the Eq. (26) with V replaced by v_C the gas flux ahead of the wave is:

$$(\rho u)_{res} = 1 + \gamma_l v_R n_l^{vap}/\sigma - \gamma_l v_C(n_l^{vap} - 1)/\sigma = const. \tag{52}$$

Ahead of the wave $X = X_{res}$ and ρu is given by (52); behind the wave $X = X_{vap}$ and ρu is given by (48). The fuel concentration in the vaporization zone is:

$$n_l^{vap} = \frac{\gamma_l v_C - \sigma X_{res}/(1 - X_{res})}{\gamma_l (v_C - v_R)}. \tag{53}$$

Ahead of the wave $\theta = 0$ and behind the wave $\theta = \theta_{vap}$, $(\rho u)_{vap}$ is given by (48). We substitute $w_r = 0$ and w_e from (30) into (25) and integrate it over the condensation wave to get:

$$\theta_{vap} \left(v_C - 1 - \gamma_l v_R n_l^{vap}/\sigma \right) = \beta v_C (n_l^{vap} - 1). \tag{54}$$

The oxygen flux does not change in the condensation wave. Similarly to the vaporization layer, this yields the condition $Y \rho u = const = Y_{unb}$. Thus, the oxygen fraction ahead of the combustion wave is $Y = Y_{unb}/\rho u$, where $(\rho u)_{res}$ is given in (52).

3.4 Defining system of equations for the wave sequence. The wave sequence (see Fig. 2) is determined by a system of nonlinear algebraic equations (36)–(38) and (49), (54). In (49) and (54) one should use θ_{vap} obtained from (50), (48) as

$$\theta_{vap} = h \big/ \log(\alpha / X_{vap}) - \theta_0, \;\; X_{vap} = \frac{1}{1 + \sigma/(\gamma_l v_R n_l^{vap})}, \tag{55}$$

and substitute n_l^{vap} from (53). Therefore, (36)–(38) and (49), (54) contain three unknowns: the combustion temperature θ_h and the wave speeds v_R, v_C. This nonlinear system must be solved numerically. In numerical calculations, it is useful to know that $v_R < Y_{inj}\sigma/\gamma_f$, which follows from (37) with $Y_{unb} > 0$. Having found θ_h, v_R and v_C, expressions (37), (48)–(50), (52) and (53) determine the other solution parameters.

4 Numerical results for typical reservoir data

Numerical computations were carried out for typical parameters of in-situ combustion with petroleum coke fuel and vaporizable oil, see [2, 15]. The dimensional parameters are given in Table 1. The corresponding reference quantities and dimensionless parameters are

$$\begin{gathered} t^* = 2.62\,\text{days},\; x^* = 0.314\,\text{m},\; T^* = 197.5\,\text{K},\; v^* = 0.120\,\text{m/day}, \\ Le = 2.175 * 10^{-2},\; N_{Da} = 2.26 * 10^{13},\; \gamma_f = 67.7,\; \gamma_l = 180.5,\; \sigma = 5.56 * 10^3, \\ \beta = 0.228,\; h = 24.7,\; \mathcal{E} = 97.4,\; \kappa = 2.26 * 10^3,\; \theta_0 = 1.48,\; \alpha = 4.83 * 10^5. \end{gathered} \tag{56}$$

Solving equations(36)–(38), (49), (54) numerically with the data (56), we obtain the wave sequence parameters given in the second row of Table 2. We can expect that the same conclusion is usually true for liquid fuels, so the liquid fuel, if available, does not participate in the combustion.

For comparison, the numerical simulation was carried out using an implicit finite difference scheme for the PDE system (14)–(19). The steady solution obtained using numerical simulation is presented in Fig. 5, where the temperature θ with the fuel concentration n_f and vaporizable

parameters	values	parameters	values
K_r	10^8 1/s	Q_r	$4.74 * 10^5$ J/mole
Q_e	$4.06 * 10^4$ $\frac{J}{mole}$	R	8.314 J/mole K
E	$1.6 * 10^5$ $\frac{J}{mole}$	P_{tot}	10^5 Pa (1 atm)
C_m	$2 * 10^6$ J/m^{3}K	Y_{inj}	0.21 $\frac{\text{mole of } O_2}{\text{mole of air}}$
λ	0.87 J/msK	D	$2 * 10^{-5}(P_{tot}/P_{atm})$ m^2/s
k	0.01 1/s	n_f^{res}	833.3 $\frac{mole}{m^3}$ ($\frac{\text{10 kg of carbon}}{m^3}$)
c_g	29.2 J/mole K	n_l^{res}	2222 $\frac{mole}{m^3}$ ($\frac{\text{10 kg of oil}}{m^3}$)
φ	0.3	T_b	373.15 K (oil)
T_{res}	293.15 K	u_{inj}	200 m/day

Table 1: Typical values of the parameters for in-situ combustion.

	θ_h	v_R	Y_{unb}	θ_{vap}	v_C	X_{vap}	n_l^{vap}
analytic	2.212	1.507	0.192	0.064	4.400	0.056	1.213
numeric	2.220	1.536	0.192	0.060	4.404	0.054	1.200

Table 2: Parameters of the wave sequence solution obtained by analytical formulae and numerical simulation.

oil concentration n_l are shown. The combustion-vaporization and condensation wave are well distinguished in the figure (the thermal wave on the left is not shown). The parameters of this solution are given in the third row of Table 2. This table shows that they are in very good agreement with the theoretical values in the second row. In other words the analytical and numerical solutions show good agreement.

5 Exact solution for dry combustion

In Section 3 we have constructed the approximated traveling wave solution for the combustion-vaporization model described by system (14)-(21). However, this solution is not exact from the mathematical point of view. In fact it is a transient solution. In this section we want to see if the solution obtained previously is close to the exact traveling wave solution for the system (14)-(21). As this system is not trivial to solve analytically, we will apply the singular perturbation method to the dry gas-solid combustion model, which can be regarded as a particular case of the original combustion-vaporization model.

In the absence of evaporation-condensation phenomena we obtain an analogous dimensionless system of equations substituting (14) by:

$$\frac{\partial \theta}{\partial t} + \frac{\partial \rho u \theta}{\partial x} = \frac{\partial^2 \theta}{\partial x^2} + w_r; \tag{57}$$

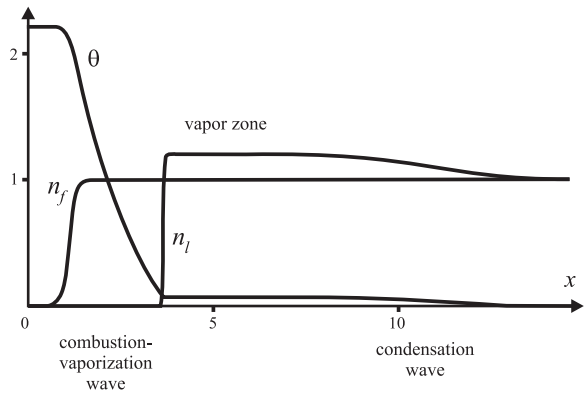

Figure 5: Results of numerical simulation for combustion-vaporization and condensation waves.

and (15) by:

$$\frac{\partial \rho}{\partial t} + \sigma \frac{\partial \rho u}{\partial x} = 0; \tag{58}$$

together with (16), (18), (20). Next we summarize the study of system (57), (58), (16), (18) and (20) as done in [8].

5.1 Combustion wave profile. In order to study the profile of the combustion wave (moving with speed V analogous to speed v_R in Fig. 2) we look for the stationary solution of (57), (58), (16), (18) and (20) in the traveling wave coordinate $\xi = x - Vt$. Next we follow [16] and we neglect the terms $-V\rho'$ and $-V(Y\rho)'$ as compared to other terms, where the prime denotes the derivative with respect to ξ. Under these simplifications, using (18), system (57), (58), (16), (18) and (20) reduces to

$$\theta'' + (V-1)\theta' = -\Phi, \tag{59}$$

$$\left(\frac{\theta_0 Y'}{\theta + \theta_0}\right)' \frac{1}{L_e} - \sigma Y' = \mu \Phi, \tag{60}$$

$$\rho_f' = \Phi / V. \tag{61}$$

$$\rho u = 1. \tag{62}$$

From (20) it follows that the reaction stops ($\Phi = 0$) when $Y\rho_f = 0$. Ahead of the wave $\rho_f = 1$, so we must have $Y = 0$. Behind the wave $Y = 1$, hence, $\rho_f = 0$. These two conditions mean that the fuel and oxygen are completely consumed in the reaction:

$$\xi \to -\infty: \quad \rho_f^b = 0,\ Y^b = 1, \qquad \xi \to \infty: \quad \theta^u = Y^u = 0,\ \rho_f^u = 1; \tag{63}$$

where the superscripts u and b mean unburned and burned states.

Substituting (61) into (59)-(60), integrating from ξ to ∞, using left boundary condition from (63) and the hypothesis that $\theta' \to 0$ and $Y' \to 0$ when $\xi \to \infty$ we obtain:

$$\theta' = (1 - V)\theta + (1 - \rho_f)V, \tag{64}$$

$$Y' = \frac{L_e(\theta+\theta_0)}{\theta_0}(\sigma Y + \mu V \rho_f - \mu V), \tag{65}$$

The equations (64), (65) together with (61) determine the travelling wave profile. Using the right boundary conditions from (63) and $\theta' \to 0$, $Y' \to 0$ when $\xi \to -\infty$ leads to the Rankine-Hugoniot relations. We can rewrite them obtaining the wave speed and the combustion front temperature:

$$V = \frac{\sigma}{\mu}, \quad \theta^b = \frac{\sigma}{\sigma - \mu}. \tag{66}$$

Note that the combustion wave speed and the burning temperature do not depend on the reservoir temperature as σ and μ are proportional to T_{res}.

5.2 Wave profile approximation. The wave profile is defined by the solution of the system (61), (64) and (65). One notices that the change of the variables θ, Y and ρ_f in ξ is of order 1 and, thus, the derivatives θ', Y' and ρ_f' are of the same order. Let us define

$$\epsilon = N_{Da} \exp(-\mathcal{E}/(\theta^b + \theta_0))/V. \tag{67}$$

We rewrite (61) using ϵ:

$$\rho_f' = \epsilon Y \rho_f \exp\left(\frac{\mathcal{E}}{\theta_b + \theta_0} - \frac{\mathcal{E}}{\theta + \theta_0}\right) \tag{68}$$

From (68) we find that $\rho_f' \leq \epsilon$. Therefore

$$\theta' \sim Y' \sim \rho_f' \lesssim \epsilon. \tag{69}$$

Notice that the terms on the R.H.S of (64) are of order $\sim V$ and the terms on the R.H.S of (65) are $\sim L_e\sigma$. We assume $\epsilon \ll V$; $\epsilon \ll L_e\sigma$. Using (69) we realize that the derivatives θ' and Y' in (64), (65) can be neglected. This gives the quasi–stationary approximation of the system (61), (64), (65):

$$\theta^0 = (1 - \rho_f^0)V/(V-1), \tag{70}$$

$$Y^0 = \mu V(1 - \rho_f^0)/\sigma, \tag{71}$$

$$\rho_f^{0\prime} = \frac{N_{Da} Y^0 \rho_f^0}{V} \exp\left(-\frac{\mathcal{E}}{\theta^0 + \theta_0}\right). \tag{72}$$

Substitute (70), (71) into (72), solve the resulting ODE leads to ρ_f^0. Next, we substitute ρ_f^0 into (70) and (71) getting the stationary approximation of the traveling wave. The result can be seen on the left side in Figures 6 and 7, where we use $\rho_f^0(\xi = 0) = \hat{\rho}_f = 0.5$

Next we notice that it is possible to find the solution of the system (64), (65), (68) in form of the asymptotic series $\theta = \theta^0 + \epsilon\theta^1 + \cdots$, $Y = \theta^0 + \epsilon Y^1 + \cdots$ and $\rho_f = \rho_f^0 + \epsilon\rho_f^1 + \cdots$. In [8] it is proved that the zero order terms in these expansions θ^0, Y^0, ρ_f^0 coincide with the quasi-stationary approximation (70)-(72), and the first order terms θ^1, Y^1, ρ_f^1 were obtained. The necessary condition to validate the asymptotic series expansion is that the first order correction terms are smaller than the zero order terms. In the right side of Figures 6 and 7 we show the first order correction terms.

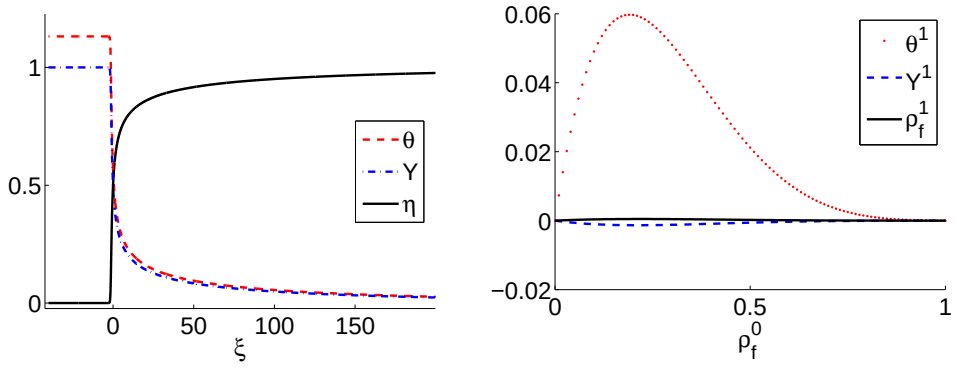

Figure 6: Stationary approximation of the combustion traveling wave on the left. First order approximation on the right. We use the parameter values $\sigma = 7.08 \cdot 10^3$, $\mu = 822.04$, $\theta_0 = 0.94$, $N_{Da} = 1.56 \cdot 10^4$, $\mathcal{E}$= 12.15 and $L_e = 2.17 \cdot 10^{-2}$.

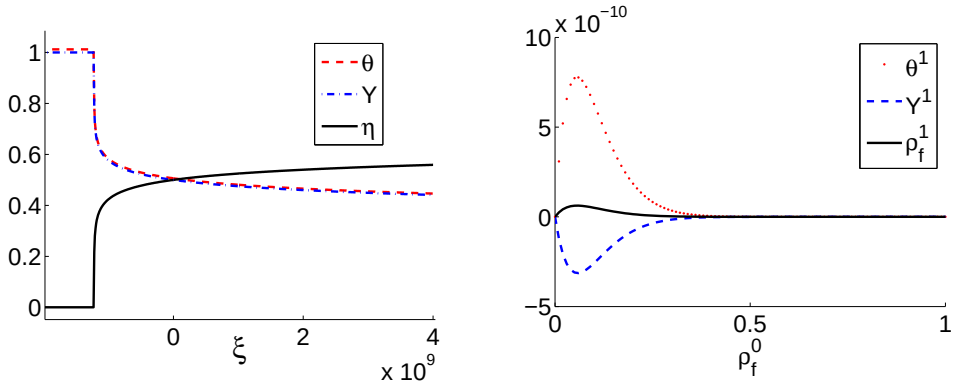

Figure 7: Stationary approximation of the combustion traveling wave on the left. First order approximation on the right. We use the parameter values given in Eq. (56).

6 Conclusions

• A model was derived for combustion of oil that allowed for oxidation of oil and evaporation of vaporizable oil.

• The form of an approximate solution based on experimental evidence was proposed, viz., as sequence of waves from the injection to the production point consisting of a thermal wave, a combustion-vaporization wave and a condensation wave.

• The traveling wave solution for the reaction zone can only be obtained under the assumption that oxidation reaction ceases below a critical oxygen concentration Y_{unb}.

• Numerical solution for short time shows good agreement with the semi-analytical solution of the oxidation-evaporation model.

• A dry gas-solid combustion model can be solved by considering traveling wave solution for the combustion front. This model shows that only for a restricted parameter set the solution for the combustion-vaporization wave is close to the dry gas-solid combustion wave.

References

[1] ABU-KHAMSIN, S. A., BRIGHAM, E. AND RAMEY, JR., H. J., *Reaction kinetics of fuel formation for in-situ combustion*, SPE Reservoir Engeneering, SPE 15736-PA, 1988.

[2] AKKUTLU I. Y. AND YORTSOS Y. C., *The dynamics of in-situ combustion fronts in porous media*, Combustion and Flame, **134** (2003), 229—247.

[3] ALDUSHIN A. P., RUMANOV I. E. AND MATKOWSKY B. J., *Maximal energy accumulation in a superadiabatic filtration combustion wave*, Combustion and Flame **118** (1999), 76—90.

[4] BOBERG, T.C., *Thermal Methods of Oil Recovery*, An Exxon Monograph Series, 1988.

[5] BIRD R.B., STEWART W.E. AND LIGHTFOOT E.N., *Transport Phenomena*, 2nd ed. Wiley, New York, 2002.

[6] BRUINING J. AND MARCHESIN M., *Nitrogen and steam injection in a porous medium with water*, Transport in Porous Media **62** (2006), 251-281.

[7] BRUINING, J., MAILYBAEV, A.A. AND MARCHESIN, D., *Filtration combustion in wet porous medium*. In preparation, 2009.

[8] CHAPIRO, G., MAILYBAEV, A. A., MARCHESIN, D., SOUZA, A. J., *Long time asymptotic solution for forward filtration combustion*, In preparation, 2009.

[9] GATES, C.F. AND RAMEY JR., H.J., *Field results of south belridge thermal recovery experiment*, Petroleum Transactions, AIME, 213:236–244, 1958. SPE 1179-G.

[10] LIDE D. R., ED., *Handbook of Chemistry and Physics*, CRC Press, Boca Raton, 2008.

[11] KORN G. A. AND KORN T. M., *Mathematical Handbook for Scientists and Engineers*, McGraw-Hill, New York, 1968.

[12] PRATS, M., *Thermal Recovery*, SPE of AIME, 1982.

[13] SCHULT D. A., MATKOWSKY B. J., VOLPERT V. A. AND FERNANDEZ-PELLO A. C., *Forced forward smolder combustion*, Combustion and Flame, **104**, 1–26, 1996.

[14] SHOOK, M. AND LI, D. AND LAKE, L.W., *Scaling immiscible flow through permeable media by inspectional analysis*, Situ, **16**, 4:311–349, 1992.

[15] SMITH I.W., *The intrinsic reactivity of carbons to oxygen*, Fuel, **57** (1978), 409-414.

[16] WAHLE C. W., MATKOWSKY B. J. AND ALDUSHIN A.P., *Effects of gas-solid nonequilibrium in filtration combustion*, Combust. Sci. and Tech., **175** (2003), 1389–1499.